ISBN: 978-3-95450-204-2 ISSN: 2673-5350 doi:10.18429/JACoW-IBIC2019-TUPP041

OBSERVATIONS OF LONG-RANGE AND SHORT-RANGE WAKEFIELD EFFECTS ON ELECTRON-BEAM DYNAMICS IN TESLA-TYPE SUPERCONDUCTING RF CAVITIES *

A.H. Lumpkin†, R. Thurman-Keup, N. Eddy, D. Edstrom, and J. Ruan
Fermi National Accelerator Laboratory, Batavia, IL 60510 USA

Abstract

The assessments of long-range and short-range wakefield effects in TESLA-type superconducting rf cavities at the Fermilab Accelerator Science and Technology Facility are described. A dipolar higher-order mode (HOM) of one cavity is shown to be in near resonance with the 3-MHz micropulse repetition frequency harmonic resulting in a clear sub-macropulse centroid oscillation of 100 kHz. In the short-range wakefield measurements, a head-tail transverse kick of ~100 μm is seen in the streak camera images with 500 pC/b and offsets of ~2 mm. A numerical model for the TESLA-type cavity is consistent with these latter results.

INTRODUCTION

Generation and preservation of bright electron beams are two of the challenges in the accelerator community given the inherent possibility of excitations of dipolar long-range wakefields (e.g. higher-order modes (HOMs)) and short-range wakefields due to beam offsets in the accelerating cavities. The Fermilab Accelerator Science and Technology (FAST) facility has a unique configuration of a photocathode rf gun beam injecting two TESLA-type single cavities (CC1 and CC2) in series prior to the cryomodule [1]. Beam propagation off axis in these cavities can result in emittance dilution within the macropulses and micropulses, respectively. Since such cavities form the drive accelerator for the FLASH FEL [2], the European XFEL[3], and the under construction LCLS-II [4], understanding the possible emittance dilution effects is of interest.

Two configurations of a Hamamatsu C5680 streak camera viewing a downstream OTR screen were utilized to track centroid shifts during the macropulse (framing mode) for the long-range case and during the micropulse for the short-range case (~10-micron spatial resolution and 2-ps temporal resolution). Steering before CC1 resulted in a bunch centroid oscillation within the macropulse attributed to a near-resonance condition of an HOM with a beam harmonic that was detected by the downstream rf BPMs and the streak camera. Steering before CC2, we observed a head-tail centroid shift in the streak camera image y(t) profiles which we attributed to a short-range wakefield effect. We will describe the potential emittance dilution effects we have seen in TESLA-type cavities due to off-axis beam trajectories.

* This manuscript has been authored by Fermi Research Alliance, LLC under Contract No. DE-AC02-07CH11359 with the U.S. Department of Energy, Office of Science, Office of High Energy Physics.
† lumpkin@fnal.gov

EXPERIMENTAL ASPECTS

The FAST Injector Linac

The FAST linac is based on the L-band rf photocathode (PC) gun which injects beam into two superconducting rf (SCRF) capture cavities denoted CC1 and CC2, followed by transport to a low-energy electron spectrometer. A Cs_2Te photocathode is irradiated by the UV component of the drive laser system described elsewhere [5]. The basic diagnostics for the studies include the rf BPMs located before, between, and after the two cavities as shown in Fig. 1. These are supplemented by the imaging screens at X107, X108, X121, and X124. The HOM couplers are located at the upstream and downstream ends of each SCRF cavity, and these signals are processed by the HOM detector circuits with the output provided online though ACNET, the Fermilab accelerator controls network. The HOM detectors' bandpass filters were optimized for two dipole passbands from 1.6 to 1.9 GHz, and the 1.3 GHz fundamental was reduced with a notch filter. The rf BPMs electronics were configured for bunch-by-bunch capability with reduced noise. At 2 nC per micropulse, the rms noise was found to be 25 μm in the horizontal axis (x) and 15 μm in the vertical axis (y) in B101 in the test with 4.5-MeV beam from the gun. The set of rf BPMS was critical for the HOM sub-macropulse beam effects. However, for the experiments on short-range transverse wakefields, we relied on a streak camera to provide the sub-micropulse spatial information.

Streak Camera Aspects

We utilized a C5680 Hamamatsu streak camera with S20 PC operating with the M5675 synchroscan vertical deflection unit that was phase locked to 81.25 MHz shown in Fig. 2. In addition, we used a phase-locked-loop C6878 delay box that stabilizes the streak image positions to about 1 ps temporal jitter over 10s of minutes. These steps enabled the synchronous summing of 50-150 micropulses or bunches (b) generated at 3 MHz by the photoinjector or the offline summing of 10-100 images to improve statistics in the sum images. We applied the principle to optical transition radiation (OTR) generated from an Al-coated Si substrate at the X121 screen location (see Fig.1) with subsequent transport to the beamline streak camera. Commissioning of the streak camera system was facilitated through a suite of controls centered around ACNET. This

ISBN: 978-3-95450-204-2 ISSN: 2673-5350 doi:10.18429/JACoW-IBIC2019-TUPP041

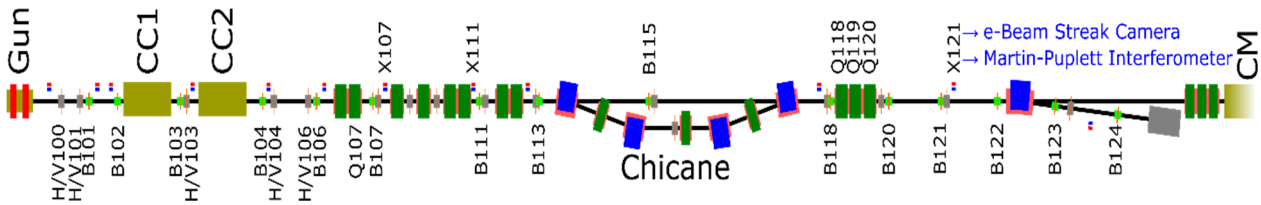

Figure 1: Schematic of the FAST linac showing the PC rf gun, H/V corrector locations, rf BPMs, CC1 and CC2 (which include two HOM detectors each), the X121 OTR station, electron spectrometer, and beginning of the cryomodule (CM).

suite includes operational drivers to control and monitor the streak camera as well as Synoptic displays to facilitate interface with the driver. Images are captured from the streak camera using the readout camera, Prosilica 1.3 Mpixel cameras with 2/3" format, and may be analyzed both online with a Java-based ImageTool and an offline MATLAB-based ImageTool processing program [6,7]. Bunch-length measurements using these techniques have been reported previously from the A0 Facility [8] and FAST first system streak camera commissioning at 20 MeV [9].

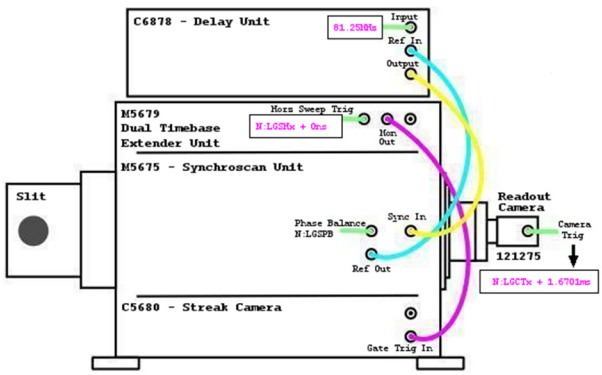

Figure 2: The Hamamatsu C5680 streak camera with synchroscan vertical sweep unit and the horizontal sweep unit. For the framing mode the slow sweep vertical unit was installed.

EXPERIMENTAL RESULTS

Long-range Wakefield (HOMs) Effects

For the long-range wakefield studies, we looked for correlations between the elevated HOM detector signals and any sub-macropulse centroid oscillations. We initially investigated vertical offsets after establishing the steering for relative HOM minima with 500 pC/b and 50b. Figure 3 shows the effects on the beam of the V101 corrector located before CC1 for settings of -1, 0, and +1 A. The 1-A values give a 10 mrad steering to the 4.5 MeV beam out of the rf gun and typically HOM signals of about 1V in the detectors. A surprisingly clear 100-kHz oscillation of the beam centroid is observed in Fig. 3 for the B107 and B113 data at z= 2.5 m and 5.0 m after CC2 with the phase changing with corrector polarity [10]. The oscillations are 2x bigger for a 10-m drift after CC2 with no quadrupoles energized as shown in Fig. 4. The oscillation amplitude was evaluated by fitting a parabola to the peaks of the oscillation in the first 50 b as indicated in Fig. 4a. The data were averaged over 100 shots for each of the 10 rf BPM locations downstream of CC2, and these amplitudes plotted vs. the z location in Fig. 4b. We then made a linear fit to the amplitudes vs. z, and reverse projected the trajectory though the cavities. The time dependent vertical kick to the beam appears to originate in CC2, and the B103 readings appear to be constant vs. the corrector current. For this charge the vertical kick angle was 40 µrad.

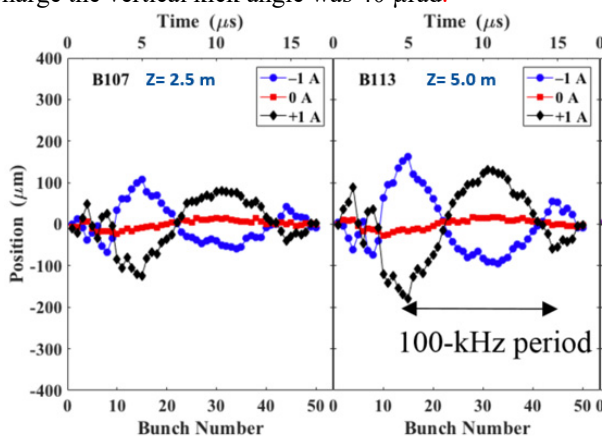

Figure 3: Readings of rf BPMs for the 50-b train for V101 corrector current values of -1, 0, and +1 A. Observations of a 100-kHz submacropulse oscillation at B107 at z=2.5 m after CC2 and B113 at z= 5.0 m after CC2 are shown [10].

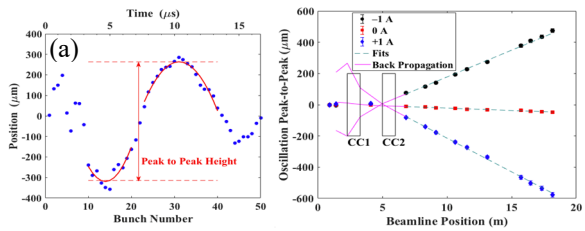

Figure 4: (a)Example of the fitting of the oscillation peaks with a parabola in the first 50 b. (b) Plot of the peak-to-peak height results for the 10 rf BPMs vs. their z position after CC2 [10].

As an additional test of the submacropulse centroid oscillation phenomenon, we utilized the X121 streak camera in framing mode. An example image is shown in Fig. 5 with a 5-µs time span vertically. Since the Q118-120 quadrupole triplet was used to match the X121 beam image into the streak camera entrance slit, the lower Beta function

ISBN: 978-3-95450-204-2 ISSN: 2673-5350 doi:10.18429/JACoW-IBIC2019-TUPP041

reduced the magnitude of the centroid oscillation at this z location. Eighteen consecutive micropulses are imaged, and by changing the trigger timing, the next set of micropulses with one micropulse overlap was obtained with the same beam conditions. The y-centroids were determined from a Gaussian fit to each of the images' projected profiles. The 35-micropulse sequence was compared to the 100-shot average rf BPM data for V101 = -1A ,+1A with 0-A data as reference. The 100-kHz oscillation is still visible in all sets of data, and the rf BPM centroid positions (solid lines) are in good agreement with the streak camera data. This is an independent diagnostic corroboration of the 100-kHz effect.

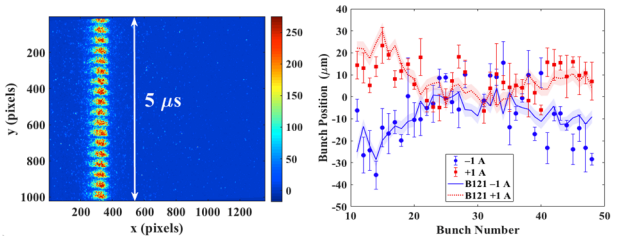

Figure 5: At left, example of framing camera mode OTR image that was analyzed for sub-macropulse beam y centroids. At right a direct comparison of the micropulse centroids extracted from the streak images for V101= -1 A (blue circles) and +1 A (red circles). and those of the rf BPMs (solid lines with error bands) [10].

The basic model for the transverse kick angle given to a micropulse due to the preceeding miropulses was described in Ref. [10]. The HOM frequencies had been measured for these two cavities, and it was found that the vertical polarization component of magnetic dipole mode 14 in CC2 had a near reasonance with the beam harmonic 623. The difference frequency was 100 kHz as in the data. The model kick angle was up to 8 μrad, and lower than the experimental result. This was still an encouraging early result and reasonable explanation of the effect.

Short-Range Wakefield Imaging Results

In Fig. 6a we show an example of the X121 OTR streak image for 50 b at 500pC/b with the "as found" steering conditions on the first run. The CC1 and CC2 detector 1 and detector 2 values were -100, -60, -100, and -50 mV, respectively. These correspond to beam offsets of about 1 mm at the entrance of both cavities based on earlier tests. The y-t space image tilt is obvious with later time upwards

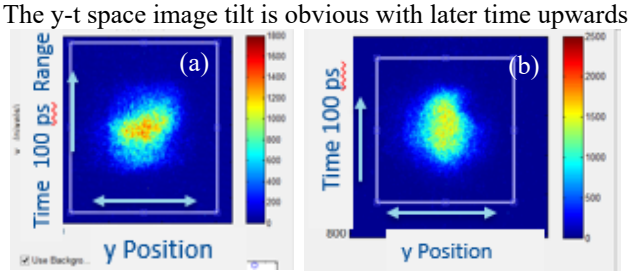

Figure 6: Streak images showing a) the y-t tilt within the micropulses when the HOMs were found elevated and b) the absence of y-t tilt when the HOM signals were minimized using the H/V101 correctors only.

in a 100-ps range and a bunch length of 11.2 ps. This can be compared to the elliptical shape (slice out of the 3-D ellipsoidal shape in a space-charge dominated regime) in Fig. 6b when the H/V 101 correctors were adjusted by about 0.5 V each to give the corresponding HOM detector values of -13, -10, -5, and -7 mV, respectively. These were ~5-mrad angle corrections. The projected y size was reduced from 548 μm to 376 μm, a notable reduction of 30% and indicate twice that for the normalized emittance. This emittance dilution is avoidable by minimizing the HOM detector signals with the concomitant reduction of the short-range wakefields.

To quantify the head-tail kicks within the micropulses, y-profiles at different time slices at the head, middle, and tail of the longitudinal profile were taken. These are shown for the initial Fig. 6a image in Fig. 7a for the head and the tail slices. The centroid shift is clear, and it is quantified with the shift of the peaks of the Gaussian fits to those profiles in Fig. 7b as δ_y=343 μm. With V103=+2.4 A change, the profiles are shown in Fig. 8 with an even larger head-tail kick of 693 μm. Using V103 = -2.4 A, the head-tail kick is only -55 μm implying that short-range wakefields in CC2 can compensate for those of CC1. The projected size is smaller than that of Fig. 6a, but the y-projection of 6b is even smaller at 376 μm.

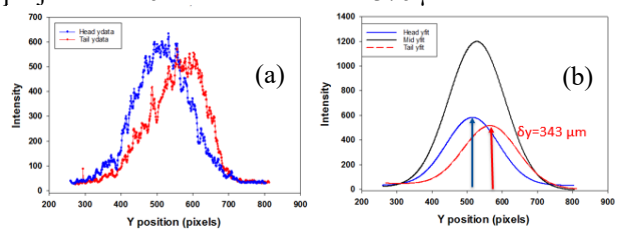

Figure 7: (a) y-profiles taken at the head and tail of the longitudinal profile. (b) the Gaussian fit profiles for the head, middle, and tail of the pulse.

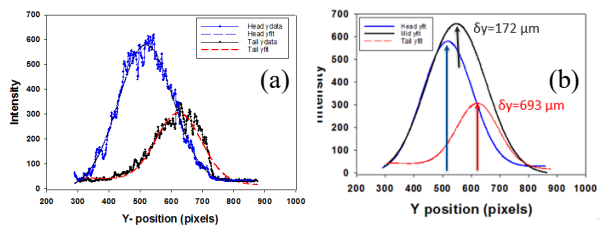

Figure 8: Example for V103= +2.4 A steering from the reference for the (a) y-profiles taken at the head and tail of the longitudinal profile and b) the Gaussian fit profiles for the head, middle, and tail of the pulse showing a head-tail shift of 693 μm.

MODELING RESULTS

A numerical model of short-range transverse wakefields in a single TESLA-type cavity shows the kick angle increases late in the micropulse as a function of time samples, s_n, as shown in Fig. 9. The input parameters were a bunch length sigma of 10 ps, a micropulse charge of 2.4 nC, an offset of 1 mm, and the M_{12} matrix element of 10 m [11]. Forty time slices are used over ± 20 ps. The calculation was done for 50 MeV so at 33 MeV at the center

ISBN: 978-3-95450-204-2 ISSN: 2673-5350 doi:10.18429/JACoW-IBIC2019-TUPP041

of CC2, the effect will be 50% larger. If we use a 5-µrad kick angle value towards the tail of the pulse and 10-m transport matrix element, we scale up this 50-µm product to a value of 75 µm. In the experiments the charge was lower at 500 pC/b in Figs. 6-8, but we expect larger offsets with 4 mrad steering with V103 and the matrix element was closer to 20 m to double the value to 150 µm. The data with two cavities involved are consistent with such shifts.

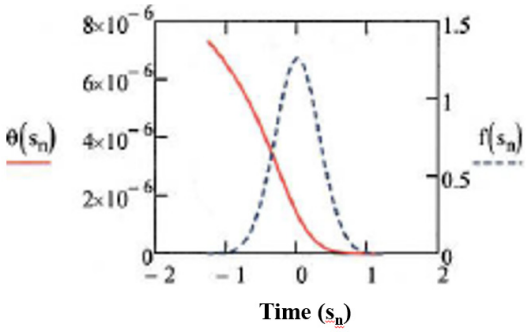

Figure 9: Example of the TESLA cavity numerical model's results for the kick angle as a function of the time slice in the micropulse (red curve) compared to the time profile of the bunch (black dashed curve). On this scale the later times are to the left, and the tail sees the biggest kick angles of 50-60 µrad.

SUMMARY

In summary, a series of observations on electron beam dynamics were made using the rf BPMs and the C5680 streak camera for the sub-macropulse and sub-micropulse time scales. The HOM detectors and rf BPMs were used to evaluate off axis steering related to these tests, and the HOM-induced sub-macropulse centroid motion was shown to be much smaller than the observed sub-micropulse effects. Moreover, the head-tail centroid kicks were consistent with a short-range transverse wakefield model for the TESLA-type superconducting rf cavities. Such considerations would be relevant in scenarios where a <1-MeV beam is injected into the first cavity and low energy is in the first three cavities of a cryomodule as planned at LCLS-II injector [12]. These wakefield-related emittance-dilution effects can be mitigated by steering on axis through the cavities as guided by the HOM signal minimizations.

ACKNOWLEDGMENTS

The authors acknowledge the short-range numerical model calculations by V. Lebedev and the support of C. Drennan, A. Valishev, D. Broemmelsiek, G. Stancari, S. Nagaitsev, and M. Lindgren at Fermilab.

REFERENCES

[1] The ASTA User Facility Proposal, Fermilab-TM-2568, October 2013.

[2] S. Schreiber, E. Schneidmiller, and M. V. Yurkov, "Recent FEL Experiments at FLASH", in *Proc. FEL'17*, Santa Fe, NM, USA, Aug. 2017, pp. 210-215. doi:10.18429/JACoW-FEL2017-TUA01

[3] H. Weise and W. Decking, "Commissioning and First Lasing of the European XFEL", in *Proc. FEL'17*, Santa Fe, NM, USA, Aug. 2017, pp. 9-13. doi:10.18429/JACoW-FEL2017-MOC03

[4] P. Emma, "Status of the LCLS-II FEL Project at SLAC", presented at the 38th Int. Free Electron Laser Conf. (FEL'17), Santa Fe, NM, USA, Aug. 2017, paper MOD01, unpublished.

[5] J. Ruan, M. D. Church, D. R. Edstrom, T. R. Johnson, and J. K. Santucci, "Commission of the Drive Laser System for Advanced Superconducting Test Accelerator", in *Proc. IPAC'13*, Shanghai, China, May 2013, paper WEPME057, pp. 3061-3063.

[6] J. Diamond, FNAL, online Java-based ImageTool, (2013).

[7] R. Thurman-Keup, FNAL, off-line MATLAB-based ImageTool (2011).

[8] A.H. Lumpkin, J. Ruan, and R. Thurman-Keup, *Nucl. Instr. and Meth. A.*, vol. 687, pp. 92-100, 2012.

[9] A. H. Lumpkin, D. R. Edstrom, and J. Ruan, "Initial Demonstration of 9-MHz Framing Camera Rates on the FAST Drive Laser Pulse Trains", in *Proc. NAPAC'16*, Chicago, IL, USA, Oct. 2016, pp. 333-336. doi:10.18429/JACoW-NAPAC2016-TUPOA25

[10] A.H. Lumpkin et al., *Phys. Rev. Accel. And Beams*, vol. 21, p. 064401, 2018.

[11] V. Lebedev (private communication, May 2016).

[12] F. Zhou, D. Dowell, P. Emma, J. F. Schmerge, C. E. Mitchell, and F. Sannibale, "LCLS-II Injector Physics Design and Beam Tuning", in *Proc. IPAC'17*, Copenhagen, Denmark, May 2017, pp. 1655-1658. doi:10.18429/JACoW-IPAC2017-TUPAB138